ACS Photonics

Letter

pubs.acs.org/journal/apchd5

Graphene–Metamaterial Photodetectors for Integrated Infrared Sensing

Isaac. J. Luxmoore,*[,†] Peter Q. Liu,[‡,§] Penglei Li,[†] Jérôme Faist,[‡] and Geoffrey R. Nash[†]

[†]College of Engineering, Mathematics and Physical Sciences, University of Exeter, Exeter, EX4 4QF, United Kingdom

[‡]Institute for Quantum Electronics, ETH Zurich, Auguste-Piccard-Hof 1, CH-8093 Zurich, Switzerland

[§]Sandia National Laboratories, Albuquerque, New Mexico 87185, United States

Supporting Information

ABSTRACT: In this work we study metamaterial-enhanced graphene photodetectors operating in the mid-IR to THz. The detector element consists of a graphene ribbon embedded within a dual-metal split ring resonator, which acts like a cavity to enhance the absorption of electromagnetic radiation by the graphene ribbon, while the asymmetric metal contacts enable photothermoelectric detection. Detectors designed for the mid-IR demonstrate peak responsivity (referenced to total power) of ∼120 mV/W at 1500 cm^{-1} and are employed in the spectroscopic evaluation of vibrational resonances, thus demonstrating a key step toward a platform for integrated surface-enhanced sensing.

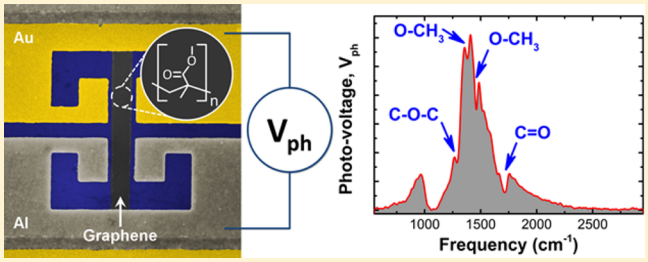

KEYWORDS: *graphene plasmonics, photothermoelectric effect, infrared, terahertz, metamaterial, biosensing, SEIRA spectroscopy*

Infrared (IR) spectroscopy is a powerful analytical technique that can be used to gain information about the chemical makeup of almost any sample in almost any state.[1] A molecular bond will absorb IR light as long as it has vibrational modes that change the electric dipole moment of the bond, and IR spectroscopy is therefore widely used across different scientific disciplines. As IR spectroscopy is both nondestructive and label-free, it is particularly attractive for the analysis of biological samples such as proteins,[2] lipids,[3] and bacteria.[4] In particular, Fourier transform infrared (FTIR) spectroscopy allows the rapid, and highly sensitive, measurement of transmission and reflection spectra. However, the large mismatch between the wavelength of light and the size of the sample of interest limits both the spatial resolution and sensitivity of such measurements.

One way to overcome this mismatch is to exploit the localized light fields associated with surface plasmon polaritons (plasmons) excited in nanostructures.[5] At mid-infrared (mid-IR) wavelengths and longer, surface plasmons are weakly bound to the metal–dielectric interface. Nevertheless, plasmonic nanostructures,[6] metamaterials,[7] and tapered waveguides[8] have been employed to confine the electric field to subwavelength volumes and significantly enhance the light–matter interaction. In contrast to noble metals, graphene has been shown to support a tightly confined surface plasmon (SP) in the THz to mid-IR spectral range,[9,10] with the significant advantage that the plasmon resonance can be tuned by changing the conductivity of graphene, which in turn can be modulated using an applied gate voltage. In very recent work, graphene plasmonic resonators have been demonstrated as an effective sensing platform,[11,12] where the tunability and strong spatial light confinement offer a tangible improvement over conventional plasmonic devices for the mid-IR sensing of protein monolayers.[12]

In this work we exploit a hybrid graphene–metamaterial[13] as a means of significantly enhancing the interaction of IR light with the sample under test, but also integrate this metamaterial with graphene photodetectors[14] operating in the IR to THz. We show that the metamaterial enhances the response of the detectors, measure a peak responsivity of >100 mV/W (defined with respect to the incident power falling on the whole area of the detector) at a frequency of ∼1500 cm^{-1}, and determine that the photoresponse is dominated by the photothermoelectric effect. Using the integrated detector we are able to reproduce the transmission spectrum of a very thin (∼20 nm) layer of test polymer, where features associated with the vibrational modes within the polymer molecules appear as minima in the measured photovoltage. This is a key step toward the realization of a fully integrated, high spatial resolution, surface-enhanced sensor and ultimately could form the basis of a spectrometer-on-a-chip.

The concept of our device is pictured in Figure 1a and b and consists of a graphene ribbon positioned in the capacitor gap of a complementary split ring resonator (CSRR), which is also split along its horizontal symmetry axis.[13] The upper and lower sections of the CSRR are in direct contact with the graphene ribbon and composed from different metals, Cr/Au (5/80 nm) for the lower section and Al (90 nm) for the upper section.

Received: April 1, 2016
Published: May 31, 2016

DOI: 10.1021/acsphotonics.6b00226
ACS Photonics 2016, 3, 936–941

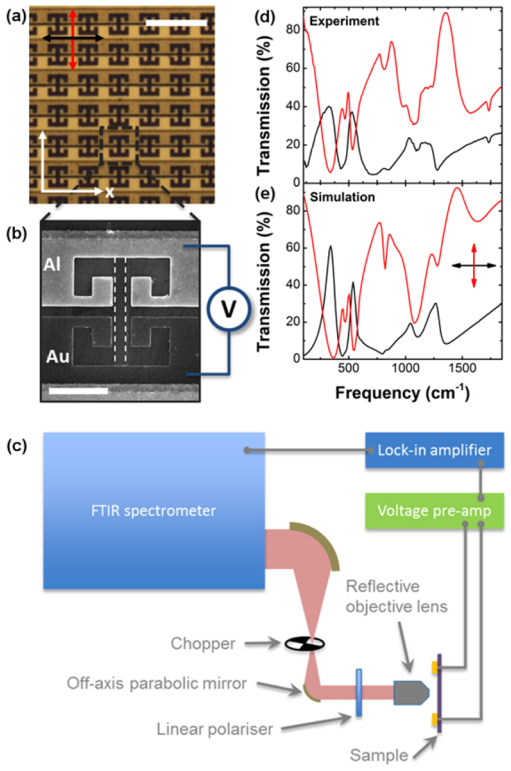

Figure 1. (a) Optical micrograph and (b) scanning electron microscope image of the hybrid metamaterial detector. The red and black arrows in (a) denote polarization parallel and perpendicular to the graphene ribbon, respectively. The dashed white lines in (b) indicate the edge of the graphene ribbon. The scale bar is 10 μm in (a) and 2 μm in (b). (c) Schematic diagram of the experimental setup. (d) Experimental and (e) FDTD simulated transmission spectra of the CSRR array without graphene ribbons. In (d) and (e) the black and red lines represent the case of perpendicular and parallel polarized excitation, respectively.

Using these two different metals has little effect on the electromagnetic response of the CSRR (see Supporting Information), but the asymmetry of the two graphene−metal interfaces facilitates photothermoelectric detection.[15] Fermi-level pinning at the graphene−metal interfaces breaks the symmetry of the carrier density and therefore the Seebeck coefficient along the graphene channel, leading to the generation of a net thermoelectric voltage. Detector arrays with an area of 600 × 600 μm^2 consist of 120 × 120 individual detector elements connected in parallel along the x-axis and in series along the y-axis as shown in Figure 1a, with source and drain contacts to allow read-out of the photovoltage and for electrical characterization of the device. In the following, we present experimental results from devices operating in two different frequency ranges. The first device, D1, targets an enhanced response in the THz range and operates across a broad frequency range. The second, D2, is designed for mid-IR operation, the optimum frequency range for vibrational spectroscopy, and is measured with and without a ∼20 nm thick layer of poly(methyl methacrylate) (PMMA) in order to investigate surface-enhanced sensing. The IR spectrum of PMMA, a versatile polymeric material, has well-known molecular absorption lines at 1730 cm^{-1} (corresponding to C═O stretching), 1450 and 1380 cm^{-1} (O−CH$_3$ bending), 1265 and 1240 cm^{-1} (C−C−O stretching), 1190 cm^{-1} (C−O−C bending), and 1145 cm^{-1} (CH$_2$ bending) and therefore provides an excellent test system.[1,16]

The detector photoresponse is measured using the experimental setup shown in Figure 1c. The broadband radiation from the FTIR is passed through a chopper wheel and a linear polarizer and then focused onto the detector (mounted inside a vacuum chamber with a KRS-5 window) using a reflective objective lens (NA = 0.5). The photovoltage generated between the source and drain contacts of the detector is amplified using a voltage preamplifier and measured with a lock-in amplifier referenced to the chopper frequency (∼500 Hz). The lock-in output voltage is then recorded as a function of the FTIR interferometer delay to record an interferogram of the detector response, the Fourier transform of which gives the spectral response of the system, i.e., the photovoltage generated due to the power spectrum of the FTIR thermal source. To quantify the performance of the detector, the photoresponse is normalized to the power spectrum of the FTIR source using a calibrated mercury cadmium telluride detector with a known spectral response (see Supporting Information). The response of D2 is further characterized using a quantum cascade laser (QCL) with a fixed frequency of ∼1200 cm^{-1}, which has a focused beam diameter of ∼60 μm (measured using a microbolometer array), considerably smaller than the detector area, and an average power of ∼8 mW.

To characterize the electromagnetic response of the hybrid metamaterial detectors, we first use FTIR spectroscopy to measure the transmission spectrum of the CSRR array (without graphene ribbons). When the incident radiation is polarized with the electric field perpendicular to the long-axis of the graphene ribbon, in the corresponding hybrid structure (see Figure 1a for orientation), the spectrum, shown in Figure 1d, reveals several peaks within the measurement frequency range of 100 to 1800 cm^{-1}. In the orthogonal polarization, with the electrical field parallel to the long axis of the graphene ribbon and also shown in Figure 1d, we observe a very different spectral response. In both cases, the spectra can be attributed to the interaction of the resonant modes of the CSRR with the optical phonons of the underlying SiO$_2$ substrate.[17] This can be shown by calculating the expected electromagnetic response using finite difference time domain (FDTD) simulations, where the optical phonons are included using a frequency-dependent dielectric function of the SiO$_2$ layer (see Supporting Information). Calculated transmission spectra are plotted for comparison in Figure 1e and show good agreement with the experimental measurements.

We then measure the photoresponse of detector D1, which is presented in Figure 2. First, we consider the response to radiation polarized perpendicular to the graphene ribbons. The photoresponse spectrum is shown in Figure 2a, recorded with $V_G \approx V_{CNP}$ (where V_{CNP} is the bias voltage corresponding to the charge neutral point). There are three main features: a broad response peak between 1500 and 4000 cm^{-1} and two narrow response peaks at ∼530 and 1250 cm^{-1}. The transmission spectrum for the perpendicular polarization is plotted in Figure 2b for comparison, and it can be seen that, in general, the photovoltage maxima correspond to the transmission maxima (the lowest frequency resonance, at ∼300 cm^{-1}, is not observed in the photoresponse because the KBr beamsplitter used in the FTIR has a cutoff frequency of 400 cm^{-1}). A similar observation is made when the polarization is parallel to the graphene ribbon, as shown in Figure 2c and d, but with a different frequency response.

DOI: 10.1021/acsphotonics.6b00226
ACS Photonics 2016, 3, 936−941

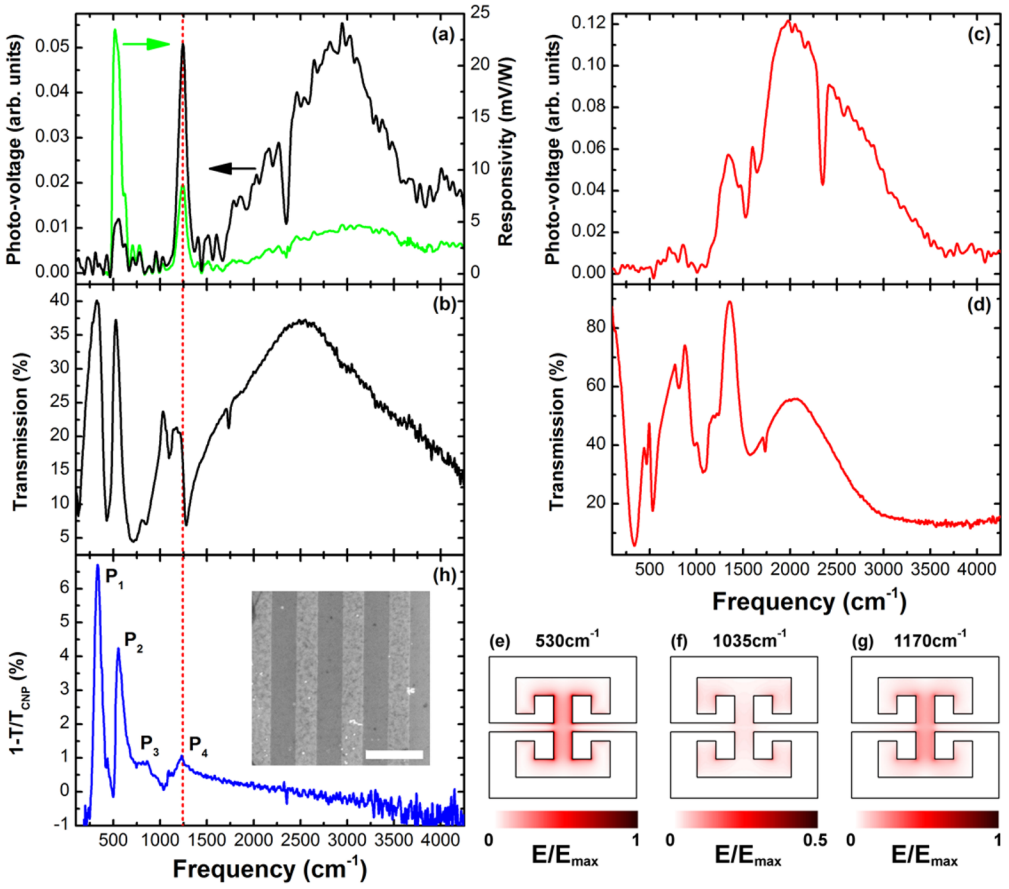

Figure 2. (a, c) Photovoltage spectra of the hybrid metamaterial detector in response to excitation with (a) perpendicular and (c) parallel polarized light. The green line in (a) shows the calibrated response spectrum. (b, d) Transmission spectra of the metamaterial array with (b) perpendicular and (d) parallel polarization. (e–g) Simulated electric field profile of the CSRR for perpendicular polarization at frequencies of (e) 530 cm^{-1}, (f) 1035 cm^{-1}, and (g) 1170 cm^{-1}. (h) Extinction spectrum of an array of 400 nm wide monolayer graphene ribbons, the plasmon–phonon modes are labeled P_1–P_4. Inset shows an SEM image of a graphene ribbon array; the scale bar is 1 μm. The red dashed line in (a), (b), and (h) indicates the frequency of the plasmon–phonon resonance in the graphene ribbon.

A correlation between the transmission and photoresponse spectra can be expected for our detector design if the CSRR confines the electric field from the incident radiation within the capacitor gap, therefore enhancing absorption within the graphene ribbon. To investigate this, we use the FDTD simulations to visualize the electric field profiles at the different resonant frequencies of the CSRR, shown for perpendicularly polarized light of three frequencies in Figure 2e–g. Enhancement of the photoresponse is observed at frequencies of 530 and 1250 cm^{-1}, which results from the strongly enhanced electric field within the capacitor gap of the CSRR as shown in Figure 2e and g, respectively. In both polarizations, however, there are resonant modes that occur in the transmission spectra but not the photoresponse; for example, in the perpendicular polarization there is no peak in photoresponse corresponding to the mode at 1035 cm^{-1}. Referring again to the FDTD simulations, we observe that in this case the resonant mode does not significantly enhance the electric field within the capacitor gap (Figure 2f). These observations provide strong evidence that the photoresponse is dominated by absorption of radiation by the graphene ribbon and enhanced by the CSRR.

We also note that the resonance in the photoresponse at 1250 cm^{-1} is significantly narrower than the transmission resonance. This is attributed to an enhanced absorption in the graphene ribbon as a result of plasmon–phonon coupling.[18,19]

The extinction spectrum ($1 - T/T_{CNP}$, where T is the transmission through the ribbon array biased to give a hole density of $\sim 1 \times 10^{13}$ cm^{-2} and T_{CNP} is the transmission through the array biased to the charge neutral point) of an array of 400 nm wide graphene ribbons (see inset to Figure 2h for SEM image) is shown in Figure 2h and shows resonant modes, labeled P_1–P_4, resulting from increased absorption due to the hybridization of the plasmon resonance in the graphene ribbons with optical phonons in the underlying SiO_2 susbstrate.[19] The plasmon–phonon mode at 1250 cm^{-1}, labeled P_4, overlaps in frequency with the CSRR mode centered at 1170 cm^{-1}, which concentrates the field within the capacitor gap, thus coupling to the graphene plasmon–phonon resonance,[13] and the enhanced absorption associated with this resonance is observed as a peak in the thermoelectric voltage.[20] This observation is supported by the line width of the plasmon–phonon mode, which is ~110 cm^{-1}, in close agreement with the ~105 cm^{-1} measured line width of the photoresponse peak. The responsivity of D1 is plotted in Figure 2a for the perpendicular polarization. A peak responsivity of 23 mV/W is measured at 530 cm^{-1}, corresponding to the LC resonance of the CSRR. Similarly, for the cavity-enhanced plasmon–phonon mode at 1250 cm^{-1} the responsivity peaks at ~9 mV/W.

We now move onto D2 and show that the combination of metamaterial with graphene detection can form the basis of an

DOI: 10.1021/acsphotonics.6b00226
ACS Photonics 2016, 3, 936–941

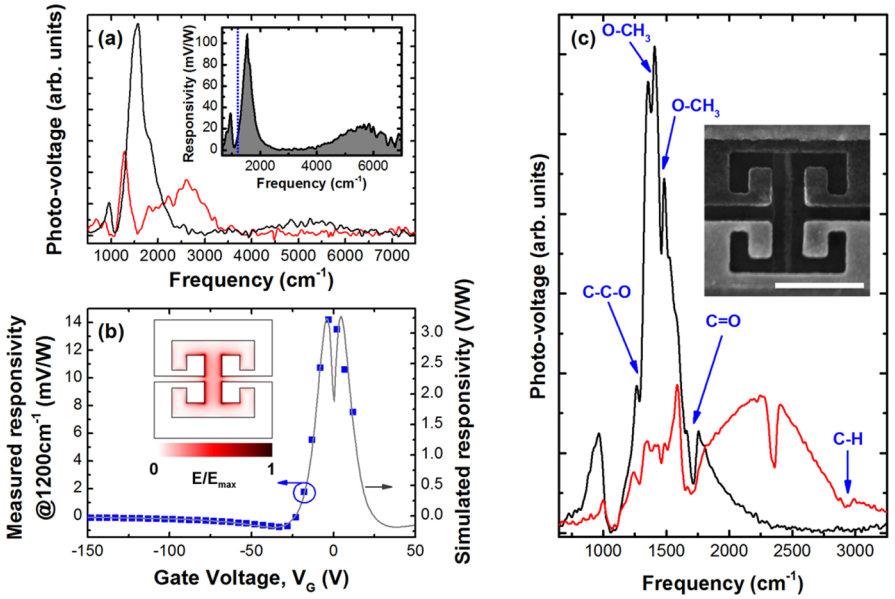

Figure 3. (a) Photovoltage spectra of hybrid metamaterial detector designed for mid-IR. The inset to (a) shows the calibrated response spectrum of the detector to perpendicular-polarized light, and the dotted blue line indicates the frequency of the QCL. (b) Experimental and calculated responsivity for the metamaterial-enhanced graphene detector as a function of gate voltage. The inset to (b) shows the calculated electric field profile of the CSRR at the QCL frequency of 1200 cm^{-1}. (c) Photovoltage spectra of the mid-IR hybrid metamaterial-enhanced graphene detector with ∼20 nm thick coating of PMMA. In (a) and (c) the black (red) line shows the response to excitation with perpendicular (parallel) polarized light. The strong absorption line at ∼2400 cm^{-1} is a result of atmospheric CO_2 absorption. The inset to (c) shows an SEM image of a single unit cell of the detector, and the scale marker is 1 μm.

integrated sensor for surface-enhanced molecular spectroscopy. D2 is designed for operation in the mid-IR with the ribbon width reduced to 200 nm and the CSRR dimensions scaled to give an LC resonance at ∼1500 cm^{-1} (see inset of Figure 3c for SEM image). The polarization-sensitive photoresponse spectra are plotted in Figure 3a, which result from the near-field enhancement of the CSRR modes, as seen previously. When the polarization is perpendicular to the graphene ribbon, the photoresponse is dominated by the LC mode of the CSRR, which hybridizes with a SiO_2 surface phonon mode, resulting in a pair of narrow resonances at ∼970 and 1550 cm^{-1}. Calibrating the response of this detector with the procedure outlined above results in a maximum responsivity of ∼110 mV/W, as shown in the inset to Figure 3a.

Figure 3b plots the responsivity of D2 to the QCL with a fixed frequency of ∼1200 cm^{-1} as a function of gate bias, which peaks at ∼12 mV/W close to the charge neutral voltage, in good agreement with the FTIR response measurement, which gives a responsivity of 13 mV/W at 1200 cm^{-1} (see inset to Figure 3a). The gate characteristic is used to identify the dominant detection mechanism as the photothermoelectric effect arising from the asymmetric metal contacts.[15,21,22] Using the FDTD simulated electric field enhancement (see inset to Figure 3b) and a one-dimensional finite element model of the carrier density and temperature distribution along the graphene channel, good qualitative agreement is found between the experimental results and the simulated responsivity, as shown in Figure 3b (see Supporting Information for simulation details). Assuming a Johnson noise floor of $\sim \sqrt{4K_BTR}$, where R is the resistance, the room-temperature noise equivalent power (NEP) can be estimated as ∼200 nW/Hz$^{1/2}$. However, the measured responsivity of the detector array is 2 orders of magnitude smaller than for a single unit cell, due to the parallel connection of the columns of detector unit cells (see Supporting Information). Therefore, we estimate that the responsivity of a single unit cell should peak at ∼1.5 V/W at 1200 cm^{-1}, in good agreement with the simulated value shown in Figure 3b, and a maximum of ∼10 V/W at 1550 cm^{-1}. This leads to a room-temperature NEP of the detector unit cell of ∼2 nW/Hz$^{1/2}$.

To investigate surface-enhanced sensing with the hybrid metamaterial detector, we deposit a ∼20 nm thick layer of PMMA directly onto the detector surface, and Figure 3c shows the modified photoresponse spectra of the detector. The detector incorporates two sensing mechanisms: refractive index sensitivity and the resonant coupling of molecular vibrations to the modes of the CSRR. First, the modification of the dielectric constant in the vicinity of the CSRR results in a red-shift of the resonant modes. This is clearly observed by comparing the resonant frequencies of the LC mode with (Figure 3c) and without (Figure 3a) the PMMA layer. The shift of ∼150 cm^{-1}, ∼10% of the resonant frequency, compares well to the refractive index sensitivity demonstrated with graphene plasmonic resonators.[11,12] Second, as shown by the photoresponse spectra in Figure 3c, for both parallel and perpendicular excitation the detector response is modified by the coupling of the resonant modes of the CSRR to the vibrational modes of the PMMA molecules. This coupling results in sharp features, which can be identified from the known vibrational resonances of PMMA as labeled in Figure 3c. Particularly clear are the C═O stretch mode at ∼1730 cm^{-1} and the bending vibration of the O−CH_3 bonds at ∼1450 cm^{-1} (ref 1). The dip in photovoltage corresponding to the frequency of the vibrational modes represents a decrease in absorption due to the destructive interference of two mutually coupled excitations in a process known as plasmon-induced transparency.[11]

DOI: 10.1021/acsphotonics.6b00226
ACS Photonics 2016, 3, 936−941

The number of C=O bonds, within the detection volume of a single CSRR, is estimated to be ~20 attomoles, following the procedure outlined by Adato et al.[23] and assuming a molecular density of 1.17 g/cm^3 and mass of 100 g/mol. The difference in the responsivity of the detector with and without the PMMA layer is estimated from Figure 3 to be ~1.2 V/W for a single unit cell, which gives a change in responsivity, $\Delta\mathcal{R}$ of 7.2×10^{16} V/Wmol. From the ratio of the Johnson noise and the change in responsivity, we then estimate an equivalent measurement noise $(\sqrt{4K_BTR}/\Delta\mathcal{R})$ of $\sim 3 \times 10^{-25}$ Wmol/Hz$^{1/2}$. This equivalent measurement noise describes the power that is required to be incident upon a single unit cell for the detection of 1 mol of material with an S/N ratio of 1 in 1 Hz bandwidth. In other words, a power of ~0.3 mW is required for a detection sensitivity of 1 zeptomole.

Finally, Figure 3c shows that the resonant response of the detector is polarization dependent, with the perpendicular polarization covering the frequency range 600−2000 cm^{-1} and the parallel polarization 1100−3000 cm^{-1}. This polarization sensitivity can provide an additional degree of freedom in identification of unknown molecules, which is highlighted by the detection of the C−H stretch mode at ~2900 cm^{-1} in the photoresponse spectrum to parallel polarization (Figure 3c).

In conclusion, we have demonstrated cavity-enhanced graphene-based photothermoelectric detectors spanning the mid-IR and THz frequency range, with broadband operation and resonant enhancement. Furthermore, the strong enhancement of the electric field combined with the electrical read-out can be used in the detection and identification of surface-adsorbed molecules, which has potential for integrated surface-enhanced sensing. An increase in responsivity of 1−2 orders of magnitude can be expected if a p−n junction is created in the graphene channel. This can be achieved by differentially doping the two halves of the graphene channel using buried or top gates or with a selective doping process, such as electron beam irradiation.[24] Importantly, this would also enable high responsivity at high carrier density in the absorption region[21,25] and therefore be compatible with enhanced absorption due to plasmonic resonances[10,18,19] and strong coupling of the hybrid metamaterial.[13] The tunability of the hybrid modes[13] also provides a route toward spectrometer-free sensing,[26] which combined with the integrated detector opens up the possibility of highly sensitive, low-cost, and miniaturized sensors for point-of-care medical applications.

■ ASSOCIATED CONTENT

Supporting Information

The Supporting Information is available free of charge on the ACS Publications website at DOI: 10.1021/acsphotonics.6b00226.

FDTD simulation details, including Lorentz model of SiO_2 permittivity; calibration of FTIR-measured photoresponse; details of photothermoelectric photoresponse model; calculation of unit cell responsivity (PDF)

■ AUTHOR INFORMATION

Corresponding Author

*E-mail: i.j.luxmoore@exeter.ac.uk.

Notes

The authors declare no competing financial interest.

■ ACKNOWLEDGMENTS

The authors thank Johanna Wolf for providing the QCL used for the detector characterization. This research was supported by the European Union under the FET-open grant GOSFEL and the Swiss National Science Foundation through NCCR QSIT. G.R.N. also gratefully acknowledges the support of the UK Engineering and Physical Sciences Research Council through a fellowship in Frontier Manufacturing (Grant No. EP/J018651/1).

■ REFERENCES

(1) Stuart, B. H. *Infrared Spectroscopy: Fundamentals and Applications*; Wiley: New York, 2004.

(2) Barth, A. Infrared Spectroscopy of Proteins. *Biochim. Biophys. Acta, Bioenerg.* **2007**, *1767*, 1073−1101.

(3) Guillen, M. D.; Cabo, N. Infrared Spectroscopy in the Study of Edible Oils and Fats. *J. Sci. Food Agric.* **1997**, *75*, 1−11.

(4) Lu, X.; Al-Qadiri, H. M.; Lin, M.; Rasco, B. A. Application of Mid-Infrared and Raman Spectroscopy to the Study of Bacteria. *Food Bioprocess Technol.* **2011**, *4*, 919−935.

(5) Kawata, S.; Inouye, Y.; Verma, P. Plasmonics for near-Field Nano-Imaging and Superlensing. *Nat. Photonics* **2009**, *3*, 388−394.

(6) Neubrech, F.; Pucci, A.; Cornelius, T.; Karim, S.; García-Etxarri, A.; Aizpurua, J. Resonant Plasmonic and Vibrational Coupling in a Tailored Nanoantenna for Infrared Detection. *Phys. Rev. Lett.* **2008**, *101*, 157403.

(7) Cubukcu, E.; Zhang, S.; Park, Y.-S.; Bartal, G.; Zhang, X. Split Ring Resonator Sensors for Infrared Detection of Single Molecular Monolayers. *Appl. Phys. Lett.* **2009**, *95*, 043113.

(8) Schnell, M.; Alonso-González, P.; Arzubiaga, L.; Casanova, F.; Hueso, L. E.; Chuvilin, A.; Hillenbrand, R. Nanofocusing of Mid-Infrared Energy with Tapered Transmission Lines. *Nat. Photonics* **2011**, *5*, 283−287.

(9) Garcia de Abajo, F. J. Graphene Plasmonics: Challenges and Opportunities. *ACS Photonics* **2014**, *1*, 133−151.

(10) Low, T.; Avouris, P. Graphene Plasmonics for Terahertz to Mid-Infrared Applications. *ACS Nano* **2014**, *8*, 1086−1101.

(11) Li, Y.; Yan, H.; Farmer, D. B.; Meng, X.; Zhu, W.; Osgood, R. M.; Heinz, T. F.; Avouris, P. Graphene Plasmon Enhanced Vibrational Sensing of Surface-Adsorbed Layers. *Nano Lett.* **2014**, *14*, 1573−1577.

(12) Rodrigo, D.; Limaj, O.; Janner, D.; Etezadi, D.; Garcia de Abajo, F. J.; Pruneri, V.; Altug, H. Mid-Infrared Plasmonic Biosensing with Graphene. *Science* **2015**, *349*, 165−168.

(13) Liu, P. Q.; Luxmoore, I. J.; Mikhailov, S. A.; Savostianova, N. A.; Valmorra, F.; Faist, J.; Nash, G. R. Highly Tunable Hybrid Metamaterials Employing Split-Ring Resonators Strongly Coupled to Graphene Surface Plasmons. *Nat. Commun.* **2015**, *6*, 8969.

(14) Koppens, F. H.; Mueller, T.; Avouris, P.; Ferrari, A. C.; Vitiello, M. S.; Polini, M. Photodetectors Based on Graphene, Other Two-Dimensional Materials and Hybrid Systems. *Nat. Nanotechnol.* **2014**, *9*, 780−793.

(15) Cai, X.; Sushkov, A. B.; Suess, R. J.; Jadidi, M. M.; Jenkins, G. S.; Nyakiti, L. O.; Myers-Ward, R. L.; Li, S.; Yan, J.; Gaskill, D. K.; et al. Sensitive Room-Temperature Terahertz Detection via the Photothermoelectric Effect in Graphene. *Nat. Nanotechnol.* **2014**, *9*, 814−819.

(16) Huth, F.; Govyadinov, A.; Amarie, S.; Nuansing, W.; Keilmann, F.; Hillenbrand, R. Nano-FTIR Absorption Spectroscopy of Molecular Fingerprints at 20 Nm Spatial Resolution. *Nano Lett.* **2012**, *12*, 3973−3978.

(17) Shelton, D. J.; Brener, I.; Ginn, J. C.; Sinclair, M. B.; Peters, D. W.; Coffey, K. R.; Boreman, G. D. Strong Coupling between Nanoscale Metamaterials and Phonons. *Nano Lett.* **2011**, *11*, 2104−2108.

(18) Yan, H.; Low, T.; Zhu, W.; Wu, Y.; Freitag, M. Damping Pathways of Mid-Infrared Plasmons in Graphene Nanostructures. *Nat. Photonics* **2013**, *7*, 394−400.

DOI: 10.1021/acsphotonics.6b00226
ACS Photonics 2016, 3, 936−941

(19) Luxmoore, I. J.; Gan, C. H.; Liu, P. Q.; Valmorra, F.; Li, P.; Faist, J.; Nash, G. R. Strong Coupling in the Far-Infrared between Graphene Plasmons and the Surface Optical Phonons of Silicon Dioxide. *ACS Photonics* **2014**, *1*, 1151−1155.
(20) Freitag, M.; Low, T.; Martin-Moreno, L.; Zhu, W.; Guinea, F.; Avouris, P. Substrate-Sensitive Mid-Infrared Photoresponse in Graphene. *ACS Nano* **2014**, *8*, 8350−8356.
(21) Song, J. C. W.; Rudner, M. S.; Marcus, C. M.; Levitov, L. S. Hot Carrier Transport and Photocurrent Response in Graphene. *Nano Lett.* **2011**, *11*, 4688−4692.
(22) Khomyakov, P. A.; Starikov, A. A.; Brocks, G.; Kelly, P. J. Nonlinear Screening of Charges Induced in Graphene by Metal Contacts. *Phys. Rev. B: Condens. Matter Mater. Phys.* **2010**, *82*, 115437.
(23) Adato, R.; Yanik, A. a; Amsden, J. J.; Kaplan, D. L.; Omenetto, F. G.; Hong, M. K.; Erramilli, S.; Altug, H. Ultra-Sensitive Vibrational Spectroscopy of Protein Monolayers with Plasmonic Nanoantenna Arrays. *Proc. Natl. Acad. Sci. U. S. A.* **2009**, *106*, 19227−19232.
(24) Yu, X.; Shen, Y.; Wu, T.; Wang, Q. J. Photodetector Based on Lateral Graphene P-N Junction Created by Electron-Beam Irradiation. *Sci. Rep.* **2015**, *5*, 12014.
(25) Gabor, N. M.; Song, J. C. W.; Ma, Q.; Nair, N. L.; Taychatanapat, T.; Watanabe, K.; Taniguchi, T.; Levitov, L. S.; Jarillo-Herrero, P. Hot Carrier-Assisted Intrinsic Photoresponse in Graphene. *Science* **2011**, *334*, 648−652.
(26) Marini, A.; Silveiro, I.; García de Abajo, F. J. Molecular Sensing with Tunable Graphene Plasmons. *ACS Photonics* **2015**, *2*, 876−882.

DOI: 10.1021/acsphotonics.6b00226
ACS Photonics 2016, 3, 936−941